THE JOURNAL OF BIOLOGICAL CHEMISTRY VOL. 286, NO. 11, pp. 9688–9698, March 18, 2011
© 2011 by The American Society for Biochemistry and Molecular Biology, Inc. Printed in the U.S.A.

# Localization of the PIP2 Sensor of TRPV1 Ion Channels*[S]

Received for publication, October 12, 2010, and in revised form, December 19, 2010 Published, JBC Papers in Press, January 11, 2011, DOI 10.1074/jbc.M110.192526

**Carmen A. Ufret-Vincenty**[1], **Rebecca M. Klein**[1], **Li Hua, Juan Angueyra, and Sharona E. Gordon**[2]
*From the Department of Physiology and Biophysics, University of Washington, Seattle, Washington 98195*

**Although a large number of ion channels are now believed to be regulated by phosphoinositides, particularly phosphoinositide 4,5-bisphosphate (PIP2), the mechanisms involved in phosphoinositide regulation are unclear. For the TRP superfamily of ion channels, the role and mechanism of PIP2 modulation has been especially difficult to resolve. Outstanding questions include: is PIP2 the endogenous regulatory lipid; does PIP2 potentiate all TRPs or are some TRPs inhibited by PIP2; where does PIP2 interact with TRP channels; and is the mechanism of modulation conserved among disparate subfamilies? We first addressed whether the PIP2 sensor resides within the primary sequence of the channel itself, or, as recently proposed, within an accessory integral membrane protein called Pirt. Here we show that Pirt does not alter the phosphoinositide sensitivity of TRPV1 in HEK-293 cells, that there is no FRET between TRPV1 and Pirt, and that dissociated dorsal root ganglion neurons from Pirt knock-out mice have an apparent affinity for PIP2 indistinguishable from that of their wild-type littermates. We followed by focusing on the role of the C terminus of TRPV1 in sensing PIP2. Here, we show that the distal C-terminal region is not required for PIP2 regulation, as PIP2 activation remains intact in channels in which the distal C-terminal has been truncated. Furthermore, we used a novel *in vitro* binding assay to demonstrate that the proximal C-terminal region of TRPV1 is sufficient for PIP2 binding. Together, our data suggest that the proximal C-terminal region of TRPV1 can interact directly with PIP2 and may play a key role in PIP2 regulation of the channel.**

TRPV1 ion channels are capsaicin-, heat-, and acid-activated non-selective cation channels expressed in nociceptors of the peripheral nervous system as well as in the neurons of the hippocampus and cortex (1). TRPV1 is an essential component of inflammatory hyperalgesia, as TRPV1 knock-out mice show essentially no hyperalgesia in response to thermal and chemical stimuli during inflammation (2). The role of TRPV1 in nociception has made it an attractive target for pain therapies. In addition, the large physical size of its pore has been shown to allow cationic local anesthetics to enter nociceptors (3), raising the possibility of identifying more specific analgesics that do not interfere with non-painful sensation.

Like many ion channels, TRPV1 is regulated by G-protein-coupled receptors (GPCR)[3] and receptor-tyrosine kinases (RTK), both of which generally sensitize nociceptors (4–5). Bradykinin, a GPCR ligand, and nerve growth factor, an RTK ligand, are released in response to tissue injury and sensitize TRPV1 to subsequent activation by noxious stimuli (6). Because both GPCRs and RTKs can activate phospholipase C (PLC), degradation of PI(4,5)$P_2$ (PIP2) by PLC was originally proposed to constitute the common mechanism for bradykinin- and nerve growth factor-mediated sensitization of TRPV1 (6). In this PLC model of hyperalgesia, PIP2 is tonically bound to TRPV1 and inhibits channel activation. Activation of PLC would decrease the concentration of PIP2 in the plasma membrane and relieve the tonic inhibition. However, a number of groups have recently shown that sensitization of TRPV1 by nerve growth factor involves facilitation of channel trafficking to the plasma membrane (7–8). The increase in the number of TRPV1 channels, rather than relief of inhibition of channels already present in the plasma membrane, appears to explain the sensitization of nociceptors in response to nerve growth factor. Further, this sensitization has been shown to require the activity of phosphoinositide 3-kinase but not phospholipase C (9), suggesting that accumulation of PI(3,4,5)$P_3$ (PIP3), and not degradation of PIP2, is the important message that mediates TRPV1 sensitization by nerve growth factor.

It has recently been shown that depletion of PIP2 in cells leads to TRPV1 channel deactivation (10, 11), indicating that PIP2 is an activator rather than an inhibitor. Furthermore, application of both short-chain and natural PIP2 to inside-out excised patches potentiates TRPV1 channels rather than inhibiting them (7, 10, 12). PIP2 appears to be tonically associated with TRPV1, as PIP2-sequestering agents such as Pleckstrin homology domains and polylysine (PolyK) (10, 12) and activation of the voltage-sensitive lipid phosphatase Ci-VSP (10) produce channel inhibition. In addition, we have shown that recruitment to the plasma membrane of a lipid phosphatase that dephosphorylates PIP2 causes inhibition of TRPV1 at both low and high concentrations of PIP2 (10) (note, however, that conflicting data on this point have been reported (12)). Thus, although the physiological role of PIP2 regulation is not yet fully understood, PIP2 is now believed to be a TRPV1 agonist, potentiating activation by chemical and thermal stimuli.

* This work was supported, in whole or in part, by National Institutes of Health Grants R01EY17564 (to S. E. G.), T32EY007031 (to R. M. K.), T32NS007332 (to C. A. U.-V.), and National Eye Institute Core Grant for Vision Research P30EY01730.

[S] The on-line version of this article (available at http://www.jbc.org) contains supplemental Figs. S1 and S2.

[1] Both authors contributed equally to the work.

[2] To whom correspondence should be addressed: Box 357290, 1959 NE Pacific St., Seattle, WA 98195-7290. Tel.: 206-616-4861; Fax: 206-685-5290; E-mail: seg@u.washington.edu.

[3] The abbreviations used are: GPCR, G-protein-coupled receptors; RTK, receptor-tyrosine kinases; DRG, dorsal root ganglion; FRET, Förster resonance energy transfer; PIP2, phosphoinositide 4,5-bisphosphate; PLC, Phospholipase C; PIP3, phosphoinositide 3,4,5-trisphosphate; PolyK, Poly-L-lysine; HBSS, Hanks' Buffered Salt Solution; IP3, Inositol 1,4,5-trisphosphate.



This is an Open Access article under the CC BY license.

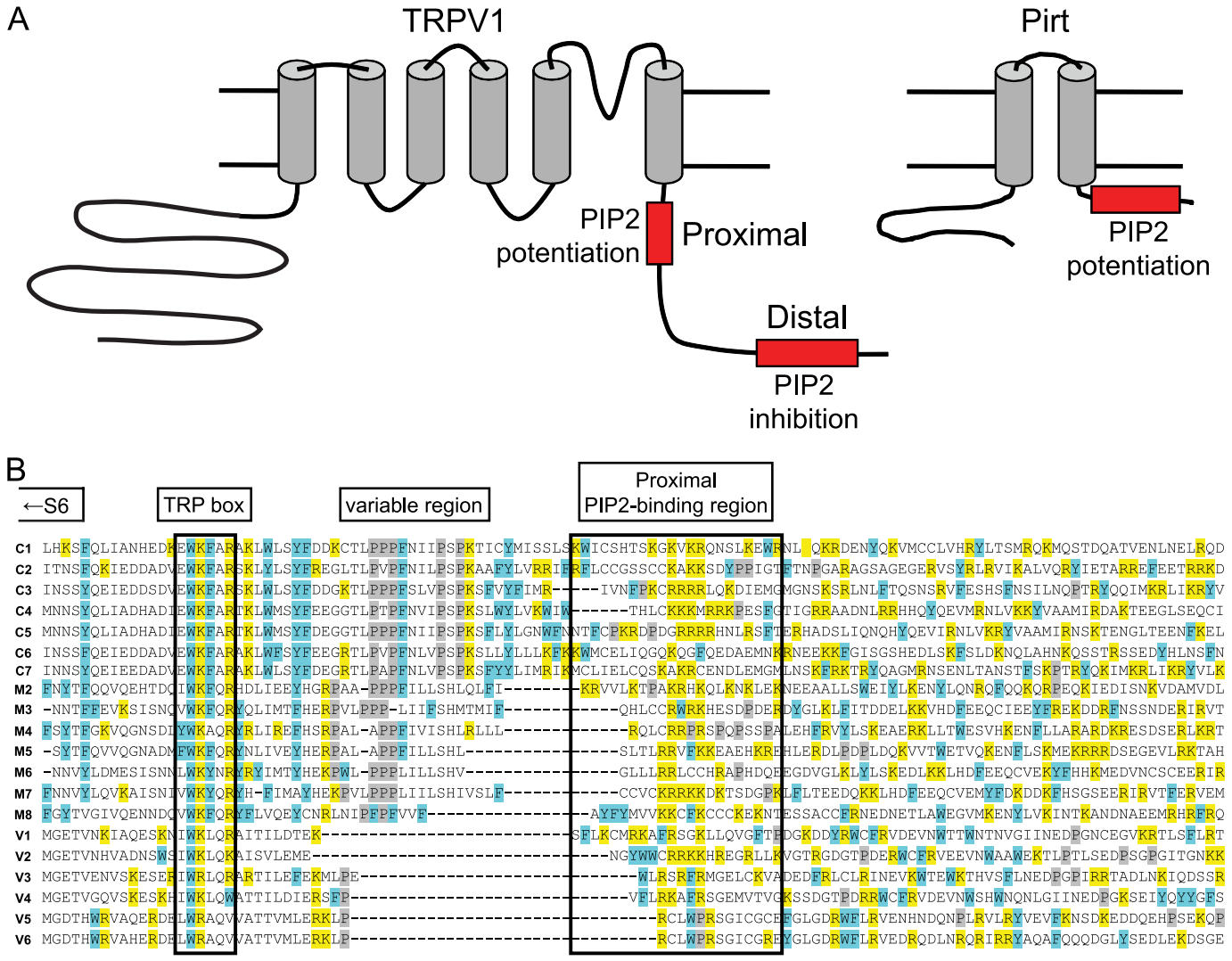


FIGURE 1. **Candidate PIP2 binding sites.** *A*, scheme of TRPV1 (*left*), highlighting two potential phosphoinositide binding sites (*red boxes*), and of Pirt (*right*) and its predicted phosphoinositide binding site (*red box*). *B*, sequence alignment beginning immediately after the putative sixth membrane spanning domain. Hydrophobic amino acids, basic amino acids, and prolines are highlighted in *blue*, *yellow*, and *gray*, respectively. From *top* to *bottom*, the initial amino acid of the shown sequences are: 611; 920; 670; 620; 624; 672; 1048; 960; 1043; 979; 1070; 1096; 979; 682; 645; 677; 718; 578; and 578. The complete sequence is not shown for any of the channels, with from 20 to 848 additional amino acids omitted between the last amino acid of the alignment and the last amino acid of the channel. The distal candidate PIP2 binding region of TRPV1 (14) would be located in these distal amino acids not shown.

Although PIP2 has been shown to regulate over 30 ion channels (13), the mechanisms by which it acts are not known. For TRPV1, even the binding site(s) for PIP2 have not yet been identified. As members of the voltage-gated family of ion channels, TRPV1 is formed as a tetramer of identical subunits, with intracellular N and C termini. Previously, a distal C-terminal region (Fig. 1*A*, *left*) was proposed to bind to PIP2, inhibiting the channels (14). Brauchi *et al.* (15) demonstrated in another study that neutralizing two basic amino acids in the proximal C-terminal region reduced PIP2 potentiation, although they did not measure whether this was due to nonspecific effects of the mutation on channel gating or to disruption of PIP2 binding. In a recently published alternative model, it was proposed that TRPV1 does not itself contain the PIP2 binding site involved in channel potentiation. Rather, Pirt (Fig. 1*A*, *right*), an integral membrane protein expressed in the same neurons as TRPV1, was proposed to act as the PIP2 sensor and in turn regulate TRPV1 activity (16).

The proximal C-terminal region represents the only cytosolic region of sequence conserved among TRPC, TRPM, and TRPV channels. This region can be divided into three sections (Fig. 1*B*): the six-amino acid TRP box; a variable region, historically known as the "TRP domain"; and a poly-basic region we propose constitutes the PIP2 binding site. As can be seen in Fig. 1*B*, the TRP box is characterized by the consensus motif (E/I/L/V/Y/F)-W-(K/R)-(F/A/L)-(A/Q)-(R/W/V). Only the W is invariant. The variable region is a proline-rich insert (Fig. 1*B*), absent in TRPV channels. The putative PIP2 binding region contains three to nine positively charged amino acids (Fig. 1*B*, *yellow*) and, typically, one or more aromatic amino acids (Fig. 1*B*, *blue*).

We addressed the localization of the PIP2 binding site on TRPV1 using a combination of electrophysiology, fluorescence spectrophotometry, and biochemistry. Our data show that neither the distal C-terminal site nor Pirt are required for potentiation of TRPV1 by PIP2. Instead, our data indicate that the

proximal C-terminal region of TRPV1 (Fig. 1, *left*) directly interacts with PIP2, making it a strong candidate for mediating regulation of the channels.

## EXPERIMENTAL PROCEDURES

*Cell Culture*—F-11 cells were cultured and transfected as described previously (7). Cells were transiently transfected with Lipofectamine-2000 (Invitrogen) according to the manufacturer's instructions and used for electrophysiology 1–4 days after transfection.

Human embryonic kidney (HEK-293) cells were cultured in DMEM supplemented with 10% FBS, 0.1 mM nonessential amino acids, 2 mM L-glutamine, and 50 units/ml penicillin with 50 $\mu$g/ml streptomycin at 37 °C and 5% $CO_2$. Cells were transiently transfected with Lipofectamine-2000 (Invitrogen) according to the manufacturer's instructions. After transfection, cells were passaged onto poly-L-lysine coated glass coverslips and grown under normal culture conditions until experimentation 24–36 h later. Note that HEK-293 cells were used only for experiments involving heterologous expression of Pirt (Fig. 4). F-11 cells or DRG neurons were used in all other cases.

*Isolation and Culture of Dorsal Root Ganglion Neurons*—DRG neurons were isolated from male wild-type and Pirt$^{-/-}$ 129/SvJ mice (generous gift from Dr. Xinzhong Dong, John Hopkins University) (16). Briefly, after euthanizing the animal, the spinal cord was removed and bisected. Whole ganglia were harvested into cold $Ca^{2+}$/$Mg^{2+}$-free Hank's Buffered Salt Solution (HBSS). Tissue was digested twice: first with 20 units/ml of papain in papain-activating solution (0.4 mg/ml L-cysteine, 1.5 mM $Ca^{2+}$, 0.5 mM EDTA in HBSS) for 20 min followed by a collagenase/dispase (1 mg/ml collagenase II and 1.2 mg/ml dispase II in HBSS) incubation for 8–15 min. Digested ganglia were triturated with a fire-polished serum-coated Pasteur pipette and resuspended into F-12 medium supplemented with 10% FBS, 50 ng/ml nerve growth factor and 50 units/ml penicillin with 50 $\mu$g/ml streptomycin. Neurons were finally plated in small volumes on glass coverslips coated with poly-L-lysine (100 $\mu$g/ml) and laminin (20 $\mu$g/ml) and placed at 37 °C and 5% $CO_2$. Two hours later, cells were flooded with fresh medium and left in culture until experimentation 24–48 h later. PCR was used to confirm the genotype of the animals (16).

*Molecular Biology*—The rat TRPV1 cDNA was a generous gift from Dr. David Julius (UCSF). The cDNA encoding Pirt was a generous gift from Dr. Xinzhong Dong (John Hopkins University). The TRPV1Δ777–820 construct was a generous gift from Dr. Gerry Oxford (Indiana University). Pirt-YFP was generated by subcloning a PCR product containing Citrine at the C-terminal end of Pirt.pcDNA3. Citrine was amplified from mCitrine.DONR221-P5P2 (a generous gift from Dr. Roger Tsien). The A206K mutation was introduced to this construct per Zacharias *et al.* (17). All cDNAs were sequenced to verify PCR product fidelity and lack of second site mutations.

*Phosphoinositides and Polylysine*—All phosphoinositides were obtained from Avanti Polar Lipids as the short-chain DiC8 versions. DiC8-$PIP_n$ solutions were solubilized in water or recording solution as a 100 $\mu$M or 1 mM stock, frozen at −20 °C, and used the same day they were diluted from the stock. Polylysine (70–150 kDa) was dissolved as a 1.2 mg/ml stock, aliquoted, and frozen at −20 °C. All other chemicals were purchased from Sigma unless otherwise noted.

*Electrophysiology*—Inside-out excised patch recordings were performed using filamented borosilicate glass pipettes heat polished with a microforge. Patch pipettes (2.5–4 MΩ for F-11 and HEK-293 cells; 3.5–4.5 MΩ for DRG neurons) were filled with saline solution (in mM: 130 NaCl, 3 HEPES (pH 7.2), 0.2 EDTA), that was also used as the external recording solution. Patches were held at 0 mV, then stepped to between −100 and +100 mV to drive the current. Solutions were delivered to the patch by positioning the pipette close to an open tube in a "sewer pipe" configuration of several tubes. The array of tubes was controlled by a RSC-200 solution-exchange manifold (Bio-Logic Science Instruments). Capsaicin was dissolved in EtOH as a 1 or 4 mM stock, then diluted to working concentrations the day of experiment. Phosphoinositide dose-response curves were recorded using either 1 $\mu$M (F-11 and DRG neurons) or 0.8 $\mu$M (HEK-293) capsaicin to elicit currents, unless otherwise noted. Currents were recorded by either an EPC-10 (HEKA) or an Axopatch 200B (Axon Instruments), controlled by Pulse (v. 8.8, HEKA) on a Dell personal computer.

*FRET Measurements in Live Cells*—Transfected HEK-293 cells were imaged on a Nikon TE-2000U inverted microscope using a Nikon ×60 oil immersion objective (numerical aperture 1.49). The microscope was coupled to an Acton Research SP-150 spectrograph (Trenton, NJ) controlled with proprietary software and a Photometrics QuantEM EMCCD camera controlled by Metamorph. Once a cell was identified, the spectrograph slit was placed over the plasma membrane region. The image of this region was projected across the grating in the spectrograph to obtain an image representing the length of the slit as a function of wavelength (bin = 4). From this image an emission spectrum of the region of interest was created using a line scan along the wavelength axis. A 440 nm solid state laser or the 488 line of an argon laser was used as an excitation source.

Spectra were analyzed using the spectral subtraction method of Zheng *et al.* (18). As controls, the emission spectra of cells expressing only CFP (440 nm excitation) or only YFP (both 440 nm and 488 nm excitation) were recorded. The CFP-only spectra were scaled to the first peak of the spectra of experimental cells and then subtracted, leaving only the YFP spectrum. This YFP spectrum contained two components, that due to direct excitation of YFP by 440 nm excitation and that due to FRET with CFP. The component due to direct excitation, called Ratio $A_0$, was calculated from cells expressing only YFP as the ratio of emission in response to 440 nm light to that in response to 488 nm light. The component due to FRET was calculated by normalizing the CFP-subtracted experimental signal to the spectrum of the experimental cells in response to 488 nm excitation. This normalized signal was called Ratio A. Any significant difference between Ratio A and Ratio $A_0$ was due to FRET. For the negative and positive FRET controls, enhanced yellow fluorescent protein (eYFP) was used. For the Pirt experiments, the YFP variant citrine was used. In the text and figures, both eYFP and citrine are referred to as YFP for simplicity.

*In Vitro FRET Assay*—Amino acids 682–725 of TRPV1 fused to CFP were inserted into the Hmal vector modified to contain a second hexa-histidine tag on the C-terminal side of maltose-

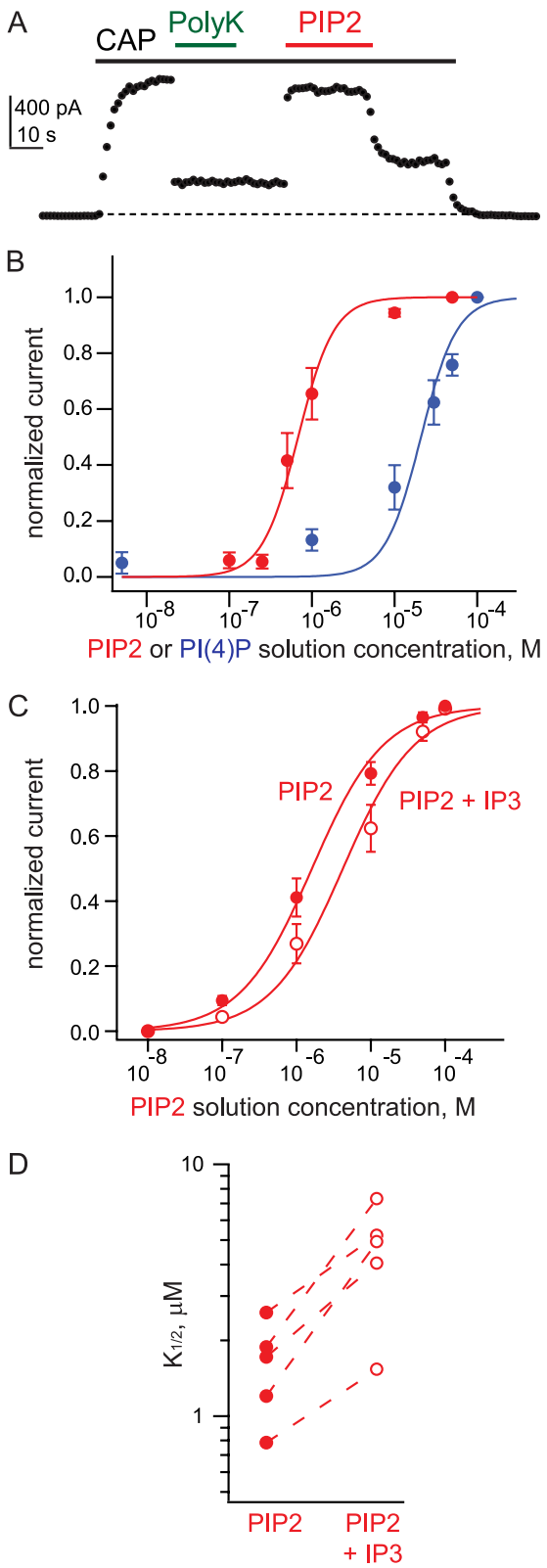


FIGURE 2. **TRPV1 modulation by PIP2.** *A*, time course of capsaicin-activated (100 nM) TRPV1 current exhibiting inhibition by PolyK and recovery from inhibition by the addition of 10 μM PIP2. The current measured at +100 mV is shown (the *dashed line* represents zero current). Note that the current did not recover upon removal of PolyK from the bath, likely because PolyK remained bound to the patch. This PolyK inhibition remained even after PIP2 was removed from the bath. *B*, dose-response curves for PI(4)P (*blue*) and PIP2 (*red*) for TRPV1. In F-11 cells, $EC_{50}$ values were 20.9 μM ($n = 5$ patches) and 0.68 μM (*red circles*, $n = 4$–7 patches), respectively and $n_H$ values obtained from the Hill fits were 2 for both curves. *C*, dose-response curves for TRPV1wt for PIP2 in the absence (*filled circles* and *line*) and presence of 10 μM IP3 (*open circles* and *line*). $EC_{50}$ values were 1.63 ± 0.3 μM and 4.6 ± 0.9 μM for without and with IP3, respectively ($n_H = 1$, $n = 5$). *D*, plot showing the increase in PIP2 $EC_{50}$ value for individual patches in the presence of IP3.

binding protein. In addition, a TEV protease site was inserted between the TRPV1 sequence and CFP. Rat TRPV2 cDNA encoding residues 645–753 fused to CFP was inserted into the same vector. The vectors were transformed into BL-21(DE3) cells and induced at 18 °C using 1 mM IPTG. Pellets from 5 ml bacterial cultures were lysed using a probe sonicator and centrifuged for 45 min at 11,000 × *g*. The supernatant was typically diluted 10–100-fold for fluorometer measurements to ensure that the fluorescence emission was within the linear range of the detector. A Jobin-Yvon Flourolog 3 was used with the following settings: 415 nm excitation with 5 nm bandwidth; emission collected between 430 and 650 nm with 5 nm bandwidth. Our analysis involved first correcting for sample dilution and then subtracting the direct excitation measured for TopFluor-PIP2 (Avanti Polar Lipids) in different experiments (Fig. 6*A*). As with the FRET experiments done in live cells, analysis of the spectra was performed in accordance with Zheng *et al.* (18).

*Data Analysis*—All electrophysiology data were analyzed with Igor Pro (Wavemetrics). Imaging data were analyzed with Metamorph and Igor Pro. In box and whisker plots, the boxes represent the range of data from the 25th to 75th percentiles, the whiskers represent the 10th and 90th percentiles and the horizontal lines represent the median. Errors given in the text and error bars shown in all figures represent the S.E. For electrophysiological measurements, all currents shown are difference currents, in which the current in the absence of capsaicin was subtracted to yield the capsaicin-activated component of the current. For the $PIP_n$ dose-response curves, the current was calculated as $I = I(\text{capsacin}+PIP_n \text{ after PolyK})/\text{Imax } PIP_n$ or $I = I(\text{capsaicin}+PIP_n \text{ after PolyK})/I(\text{capsaicin initial})$. Smooth curves shown in dose-response relations are fits of the data to the Hill equation: $I = I_{max}\ ([\text{ligand}]^n/(EC_{50}{}^n + [\text{ligand}]^n))$, where n was constrained to 1, unless otherwise noted. Statistical significance was assayed with the two-tailed Student's *t* test or with a one-way ANOVA, as appropriate.

## RESULTS

We have previously shown that TRPV1 ion channels expressed in the DRG-derived F-11 cell line can be inhibited by the application of a PIP2-specific Pleckstrin homology domain protein to the cytoplasmic side of inside-out excised patches, indicating that the channels are regulated by PIP2 in living cells and that this regulation is intact after patch excision (10). In inside-out excised patches, PIP2 potentiation can be removed by applying the PIP2-scavenger PolyK (Fig. 2*A*). Application of new PIP2 to the cytoplasmic surface of the membrane via addition to the bath can then restore potentiation (Fig. 2*A*) (10, 12).

Regulation by phosphoinositides was dose-dependent and specific, as PIP2 (Fig. 2*B*, *red circles*) was effective at solution concentrations about ten times lower than PI(4)P (Fig. 2*B*, *blue circles*). We measured dose response relations in inside-out excised patches by first measuring the capsaicin-activated cur-

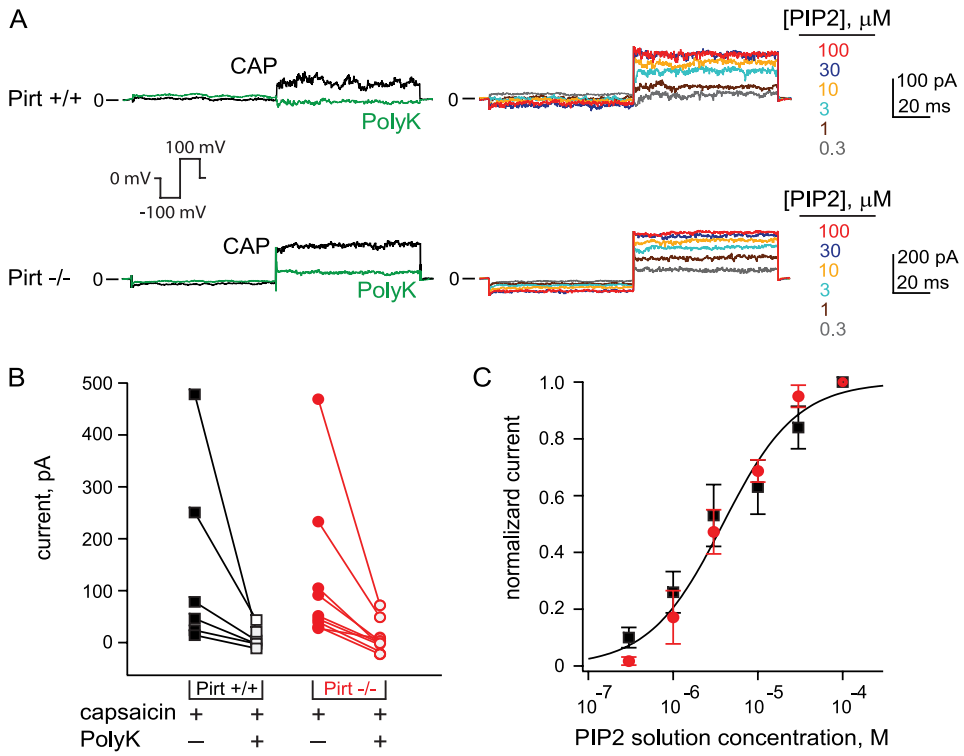


FIGURE 3. **PIP2 does not require Pirt to potentiate TRPV1 in DRG neurons.** *A*, representative data obtained using inside-out excised patches from wild-type ($Pirt^{+/+}$, *top row*) and $Pirt^{-/-}$ (*bottom row*) DRG neurons. The voltage protocol applied to obtain these data is shown. The *left column* shows TRPV1 currents measured after the addition of 1 $\mu$M capsaicin (*black*). PolyK inhibits TRPV1 currents in $Pirt^{+/+}$ and $Pirt^{-/-}$ patches (*green line*). PIP2 is able to recover TRPV1 currents after inhibition by PolyK, as shown in the *right column*. A color legend is used to represent the different concentrations of PIP2 used to measure the dose-response curves (see figures). Note that both PolyK and PIP2 were added in the presence of capsaicin, as in Fig. 2. *B*, PolyK inhibits capsaicin-activated TRPV1 currents in inside-out excised patches from DRG neurons of $Pirt^{+/+}$ (*black*, $n = 6$ patches) and $Pirt^{-/-}$ (*red*, $n = 9$ patches) mice. The current measured at +100 mV is plotted. *Filled symbols* represent the capsaicin-activated TRPV1 current. *Open symbols* represent the current measured after addition of PolyK. *C*, dose-response curves for PIP2 potentiation of capsaicin-activated TRPV1 currents in inside-out excised patches from DRG neurons of wild-type (*black*) and $Pirt^{-/-}$ (*red*) mice. $EC_{50}$ values were 3.5 ± 0.6 $\mu$M ($n_H = 1$, $n = 5$ patches) and 3.9 ± 0.5 $\mu$M ($n_H = 1$, $n = 5$ patches), respectively.

rent and then sequestering endogenous PIP2 with PolyK. After washout of the PolyK from the bath, various concentrations of either PIP2 or PI(4)P were applied via our perfusion apparatus to the intracellular surface of the patch. No ATP was present in these solutions, so that no contribution is expected from phosphorylation of the lipids by lipid kinases. The higher apparent affinity of PIP2 compared with PI(4)P could arise from either a higher affinity of TRPV1 for PIP2 binding or a more effective coupling of bound PIP2 to the activation gate. Our experiments did not distinguish between these mechanisms.

PIP2 is comprised of two distinct regions, an anionic head group and a pair of fatty acid tails. We hypothesized that anchoring a segment of the channel to the membrane might be involved in potentiation by PIP2. If this is the case, we might be able to disrupt PIP2 actions using an analog of its headgroup to compete it off the channels. To test this hypothesis, we applied inositol trisphosphate (IP3) to inside-out excised patches from cells expressing TRPV1. Concentrations of IP3 higher than 10 $\mu$M disrupted patch integrity. However, 10 $\mu$M IP3 shifted the dose-response relation for activation by PIP2 toward higher concentrations (Fig. 2*C*). For 5 out of 5 patches (Fig. 2*D*), IP3 produced a statistically significant increase (186% ± 46%) in the $EC_{50}$ for PIP2, consistent with a competitive inhibition of PIP2 by IP3. No effect of IP3 on leak currents measured in the absence of capsaicin was observed.

*Pirt Is Not Required for PIP2 Regulation of TRPV1*—It has recently been reported that the integral membrane protein Pirt (Fig. 1*A*, *right*) binds phosphoinositides and may act as the PIP2 sensor for TRPV1 (16). Capsaicin-activated whole cell currents were about half the size in dissociated dorsal root ganglion (DRG) neurons from Pirt knock-out ($Pirt^{-/-}$) mice compared with wild-type mice. Importantly, $Pirt^{-/-}$ mice were deficient in inflammatory hyperalgesia, similar to TRPV1 knock-out mice.

To test if PIP2 is able to regulate TRPV1 in the absence of Pirt, we isolated and cultured DRG neurons from wild-type and $Pirt^{-/-}$ mice. As in Fig. 2, we measured dose response relations of PIP2 added to the cytosolic side of excised patches. Representative data are shown in Fig. 3*A*. After the initial response to capsaicin (Fig. 3*A*, *black*), PolyK was added to remove the endogenous PIP2 bound to TRPV1 (Fig. 3*A*, *green*). PolyK addition inhibited capsaicin-activated currents by the same amount in wild-type and $Pirt^{-/-}$ cells (Fig. 3*B*). The fact that the PIP2-scavenger PolyK retains its ability to inhibit capsaicin-activated currents in $Pirt^{-/-}$ patches indicates that PIP2 present in the membrane after patch excision can modulate TRPV1 even in the absence of Pirt. More importantly, in patches from $Pirt^{-/-}$ cells (Fig. 3*A*, *right column*; Fig. 3*C*, *red symbols*), PIP2 added to the cytosolic side of the patches (after sequestration of endogenous PIP2 by PolyK) potentiated TRPV1 currents in a dose-dependent manner and with an apparent affinity that was not different from that measured in patches from wild-type cells (Fig. 3*C*, *black*). Neither PolyK nor PIP2 produced any changes in current when added to excised patches insensitive to capsa-

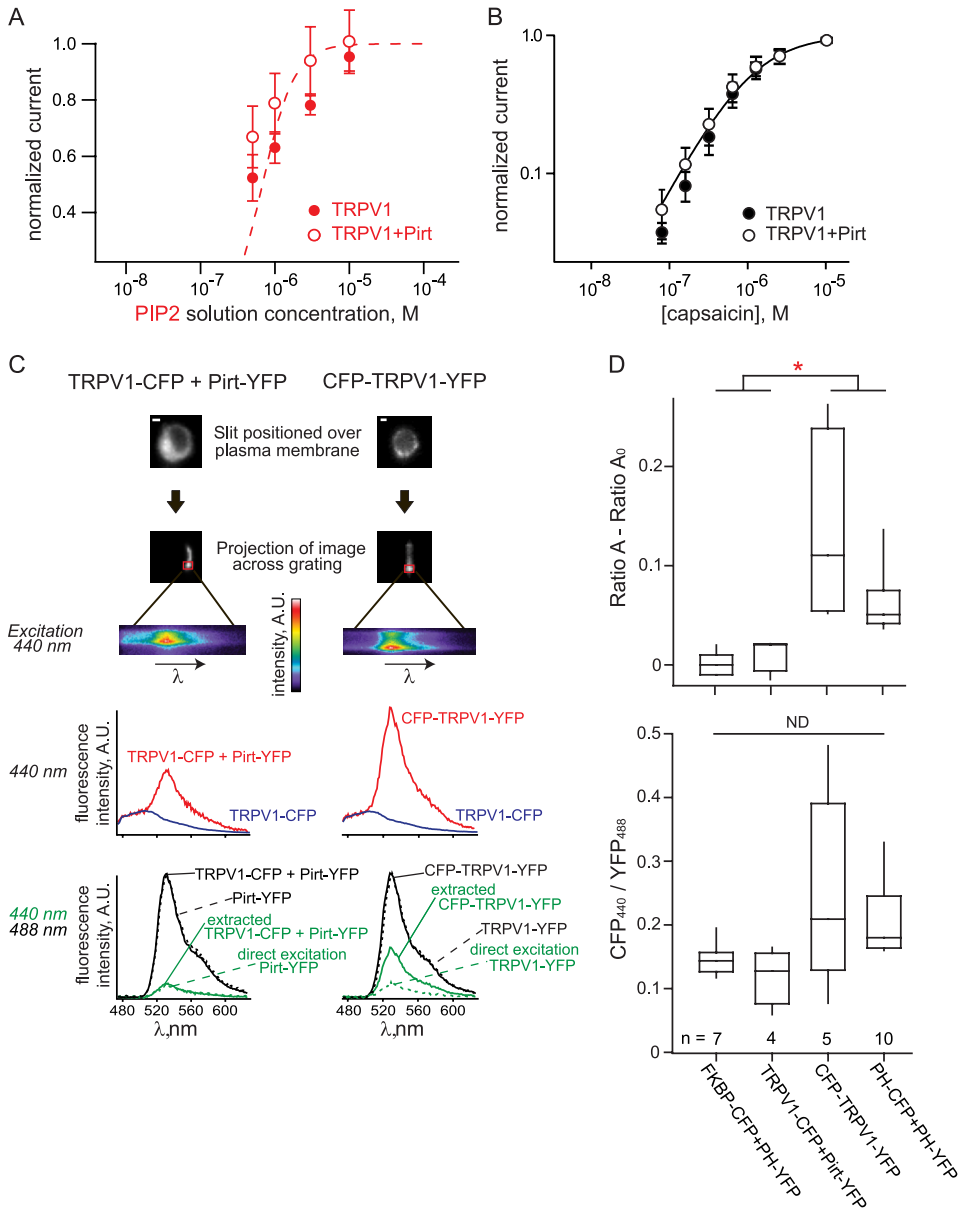


FIGURE 4. **Pirt does not appear to be involved in PIP2 regulation of TRPV1 in HEK-293 cells.** *A*, dose-response relations for potentiation by PIP2 of TRPV1 without (*filled circles*) or with (*open circles*) co-transfection of Pirt. $EC_{50}$ values were 0.60 ± 0.2 μM ($n = 6$ patches) and 0.40 ± 0.1 μM ($n = 5$ patches), respectively and $n_H$ values obtained from the Hill fits were 2 for both curves. The *dashed curve* is from the fit to F-11 cell data from Fig. 2*B*. *B*, dose-response relations for activation of TRPV1 by capsaicin either without (*filled circles*) or with (*open circles*) co-transfection with Pirt. Data from HEK-293 cells. $EC_{50}$ values were 1.08 ± 0.08 μM ($n_H = 1$, $n = 7$ patches) and 0.97 ± 0.05 μM ($n_H = 1$, $n = 7$ patches), respectively. *C*, upper: representative images of HEK-293 cells transfected with TRPV1-CFP and Pirt-YFP (*left*) or CFP-TRPV1-YFP (*right*). The *scale bars* represent 1 μm. *Middle*: a slit was positioned over the plasma membrane and the emission spectrum of a projected image of this area was obtained (pseudocolor, the abscissa of the projected spectral image is aligned with the traces below). *Lower*: emission spectra for the above images (red, 440 nm excitation) and scaled emission spectra from different cells expressing just CFP (blue, 440 nm excitation). The CFP emission (*blue*) was subtracted from the *red trace* to obtain the YFP emission (*green solid lines*). The spectra obtained when exciting YFP (488 nm excitation) in the same cells where the *red spectra* was obtained is shown in *black* (*solid lines*). Ratio A represents the maxima of the *green solid lines* divided by the maxima of the *black solid lines*. The *dotted lines* represent the emission spectra obtained from cells transfected with either Pirt-YFP (*left*) or TRPV1-YFP (*right*) when excited with 440 nm (*green*) and 488 nm (*black*) light. Ratio $A_0$ is obtained from the dotted traces similarly to Ratio A. *D*, a statistically significant difference between ratio A and ratio $A_0$ is interpreted as FRET. This difference is shown for cells transiently transfected with: FKBP-CFP and PH-YFP (negative control); TRPV1-CFP and Pirt-YFP; CFP-TRPV1-YFP (positive control); or PH-CFP and PH-YFP (positive control). TRPV1-CFP + Pirt-YFP was not significantly different than the negative control, but was different from the positive controls (for CFP-TRPV1-YFP, $p = 0.03$; for PH-CFP + PH-YFP, $p = 0.01$). The ratio of CFP:YFP intensity was not different among the four groups of cells (FKBP-CFP and PH-YFP; TRPV1-CFP and Pirt-YFP; CFP-TRPV1-YFP; PH-CFP and PH-YFP). CFP intensity was taken as the emission from 474 to 499 nm in response to 440 nm excitation. YFP intensity was taken as the peak emission in response to 488 nm intensity. ANOVA analysis of the data gave an F-value of 2.931 which is less than the $F_{critical}$ value of 3.049.

icin (data not shown). Together, these data show that in DRG neurons PIP2 does not require Pirt to activate TRPV1.

HEK-293 cells were shown not to express Pirt and heterologous expression of Pirt in HEK-293 cells enhanced the amplitude of TRPV1 whole cell currents (16). Using HEK-293 cells transfected with either TRPV1 or TRPV1 + Pirt, we asked whether the presence of Pirt influences the ability of PIP2 to regulate TRPV1. We found that co-transfection of Pirt with TRPV1 (Fig. 4*A*, *open circles*) yielded channels with the same apparent affinity for PIP2 as those from cells transfected with

only TRPV1 without Pirt (Fig. 4*A*, *filled circles*). As well, no difference in the apparent affinity for capsaicin was observed in patches from HEK-293 cells transfected with only TRPV1 (Fig. 4*B*, *filled circles*) compared with patches from HEK-293 cells transfected with both TRPV1 and Pirt (Fig. 4*B*, *open circles*).

The Pirt hypothesis predicts that Pirt and TRPV1 will lie in close proximity and may even form a protein complex (16). To test this hypothesis, we used Förster Resonance Energy Transfer (FRET) in HEK-293 cells. FRET is the non-radiative transfer of energy that can occur between two nearby fluorophores if the emission spectrum of one (donor) coincides with the excitation spectrum of the second (acceptor). How close the two molecules must be for a donor fluorophore to relax from an excited state by the radiationless transfer of its energy to an acceptor molecule is determined by the degree of overlap of the donor emission and acceptor excitation spectra, in addition to other factors. The distance at which a donor-acceptor pair exhibits 50% FRET efficiency is called the Förster radius. For the fluorophores used here, cyan fluorescent protein (CFP, donor) and yellow fluorescent protein (YFP, acceptor), the Förster radius is about 50 Å (19).

We genetically fused CFP to TRPV1 and YFP to Pirt. If the fluorescent protein tags on Pirt and TRPV1 are separated by about the Förster radius evidence of proximity between Pirt and TRPV1 may be observed with FRET. As a negative control we used the membrane-associated Pleckstrin homology domain from phospholipase Cδ1 fused to YFP (PH-YFP) and a cytosolic FKBP protein fused to CFP (FKBP-CFP). As positive controls, we used TRPV1 subunits with CFP at the N terminus and YFP at the C terminus as well as PH-YFP co-expressed with PH-CFP (12, 20).

Images of cells typical of those used to detect FRET are shown in Fig. 4*C* (*upper panels*). To record fluorescence spectra, we positioned a cell in the slit of a spectrograph (Fig. 4*C*, *second from top*) so that the region in the slit was projected through a grating and recorded using an EMCCD camera (Fig. 4*C*, *third from top*). A line scan along the wavelength axis from the region of interest corresponding to the presumed plasma membrane was used to graph the fluorescence spectra (Fig. 4*C*, *traces*). We used the spectral subtraction method of Zheng *et al.* (18) to determine whether FRET occurred between donor and acceptor molecules. Briefly, in a sample that contains both the donor and the acceptor, the spectral subtraction method isolates the FRET signal, if present, from the donor and acceptor emission signals not due to FRET.

The ratio of total YFP emission obtained with 440 nm excitation light compared with the emission obtained with 488 nm excitation light was measured in cells expressing only YFP (440 nm:488 nm, ratio $A_0$). Ratio $A_0$ was used as a measure of the direct excitation of YFP by 440 nm light we could expect in cells where both CFP and YFP were present (Fig. 4*C*, ratio of the *dashed green traces* to the *dashed black traces*). If the ratio of the 440 nm: 488 nm YFP emission in a sample containing CFP and YFP (Fig. 4*C*, ratio of the *green solid traces* to the *black solid traces*; ratio A) exceeded that of cells expressing only YFP, the extra YFP emission was attributed to FRET. To isolate the needed YFP signals, a scaled CFP signal (Fig. 4*C*, *blue traces*) was subtracted from the experimental signals in response to 440 nm light (Fig. 4*C*, *red traces*). The resulting difference traces could then be compared with that expected from direct excitation of YFP by the 440 nm light (*i.e. green solid traces* compared with *green dashed traces* in Fig. 4*C*; Fig. 4*D*, *top*, ratio A-ratio $A_0$).

As shown in Fig. 4, *C* and *D*, no FRET was observed between TRPV1-CFP and Pirt-YFP. This can be seen from the overlap of the extracted YFP signal from the TRPV1-CFP + Pirt-YFP experiment to that of the signal representing direct excitation of YFP (Fig. 4*C*, *left*, *green solid versus green dashed traces*; Fig. 4*D*, *top*). Our negative control, FKBP-CFP (cytosolic) and PH-YFP (membrane associated), also did not exhibit FRET (Fig. 4*D*, *top*). In contrast, a robust FRET signal was observed between CFP and YFP fused to either end of TRPV1 subunits (Fig. 4, *C*, *right* and *D*, *top*). In this case, the YFP signal extracted from the CFP-TRPV1-YFP experiments significantly exceeded that expected from direct excitation of YFP by the 440 nm light (Fig. 4*C*, *right*, *green solid versus green dashed traces*; Fig. 4*D*, *top*). A second positive control, in which cells were transfected with both PH-CFP and PH-YFP fusions, also produced robust FRET (Fig. 4*D*, *top*), consistent with previous reports (12, 20).

The lack of FRET in our experiments with TRPV1 and Pirt was not due to a difference in the fluorescence intensities of CFP compared with YFP among our different experimental and control groups. As shown in Fig. 4*D* (*bottom*), this CFP:YFP ratio was not different among the groups. Given the laser power used for each excitation wavelength and the expected brightness of CFP and YFP (21), the number of CFP molecules compared with YFP molecules in our experiments ranged from about 1:2 to about 2:1. This range is near optimal for detecting FRET if it occurs. A lack of FRET may reflect a number of factors, perhaps the most important is the structural arrangement of the fluorophores on the proteins of interest. Thus, although we cannot conclude that TRPV1 and Pirt are farther apart than the Förster radius of CFP and YFP, we see no evidence that an association between them is present or is required for PIP2 regulation.

Interestingly, CFP fused to the N-terminal of a TRPV1 subunit showed FRET with a YFP fused to the C-terminal. We cannot distinguish whether that FRET occurred between fluorescent proteins of the same subunit, between fluorescent proteins of two different subunits within a channel, or both. The FRET does place the fluorescent proteins at the termini within about 50 Å of each other.

*The Distal C terminus Is Not Required for Regulation by PIP2*—We hypothesized that PIP2 binds directly to TRPV1, producing the potentiation of function observed in Fig. 2*A*. Further, we hypothesized that the conservation of function among TRP channels that produces PIP2 regulation in members of the TRPC, TRPM, and TRPV families arises from a conserved mechanism. As discussed previously, the proximal C-terminal region is the only region with sequence similarity between TRPC, TRPM, and TRPV channels (Fig. 1*B*). Thus, we propose that the polybasic/hydrophobic domain in the proximal C-terminal region may be involved in PIP2 regulation for a number of TRP channel types.

A second polybasic/hydrophobic region (residues 770–791) in the distal C-terminal region of TRPV1 (Fig. 1*A*, *left*) was

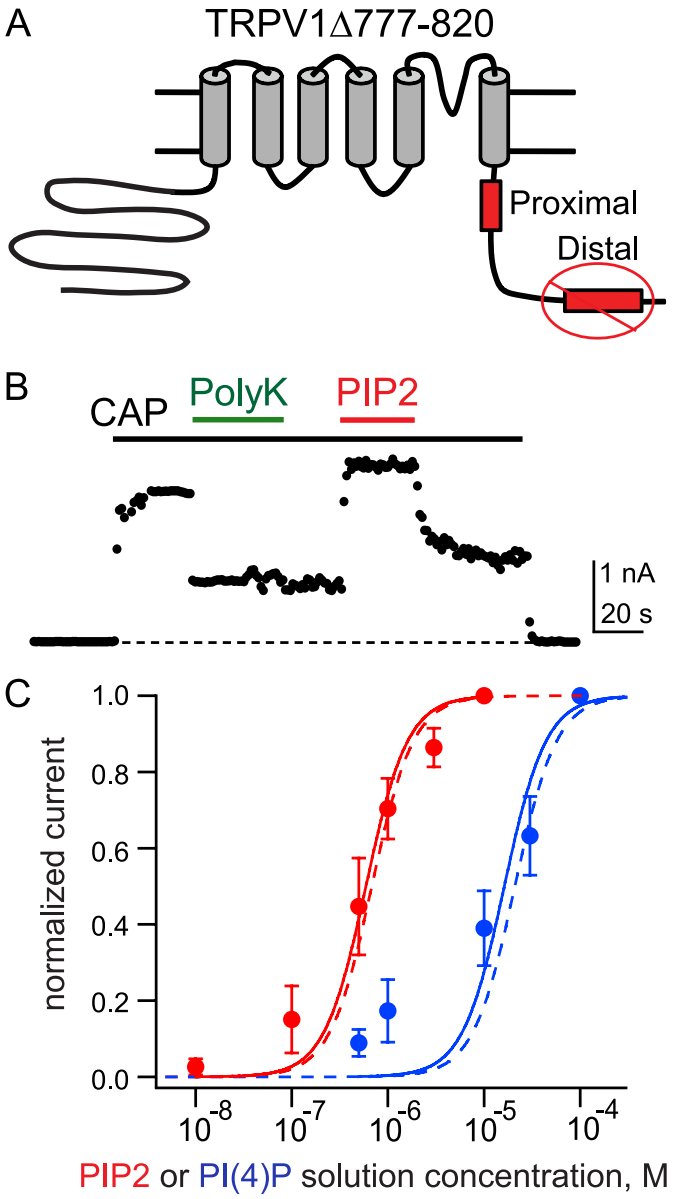


FIGURE 5. **Deletion of distal candidate phosphoinositide binding site does not remove PIP2 effect on TRPV1.** *A*, TRPV1Δ777–820 lacks the predicted distal binding site for phosphoinositides. *B*, time course of capsaicin-activated (100 nM) current for TRPV1Δ777–820. PolyK inhibits the current and this inhibition is reversed by the addition of PIP2 (10 μM). The current measured at +100 mV is shown (the *dashed line* represents zero current). *C*, dose-response curves for PIP2 (*red circles*, *solid line*) and PI(4)P (*blue circles*, *solid line*) for TRPV1Δ777-820 with the PIP2 (*dashed red line*) and PI(4)P (*dashed blue line*) fits shown for TRPV1. $EC_{50}$ values for TRPV1Δ777–820 were 0.59 ± 0.07 μM ($n_H$ = 2, $n$ = 6) and 16.3 ± 3 μM ($n_H$ = 2, $n$ = 4) for PI(4,5)$P_2$ and PI(4)P, respectively.

proposed to inhibit gating of TRPV1 upon binding of PIP2 (14). To examine whether the distal C-terminal region is required for the potentiation of capsaicin-activated currents we observed, we used a channel in which the candidate PIP2 binding site was deleted (TRPV1Δ777–820; Fig. 5*A*). As shown in Fig. 5*B*, TRPV1Δ777–820 channels were inhibited by PolyK and potentiated by PIP2. Quantification of the magnitude of PolyK inhibition and PIP2 potentiation showed no significant difference compared with wild-type TRPV1 (data not shown). In addition, the amplitudes of the TRPV1Δ777–820 patch currents in response to saturating concentrations of capsaicin were not different from wild-type TRPV1 (data not shown).

A comparison of the apparent affinity for PIP2 and specificity for PIP2 over PI(4)P for TRPV1Δ777–820 (Fig. 5*C*, *symbols*) revealed that both properties were indistinguishable from wild-type TRPV1 (Fig. 5*C*, *dashed lines*). These data indicate that the distal C-terminal region is not required for potentiation of TRPV1 by PIP2.

*Role of the Proximal C Terminus*—Hilgemann proposed that PIP2 regulation of ion channels may be mediated by displacement of a PIP2 binding site toward the plasma membrane via an electrostatic interaction between the anionic PIP2 and basic amino acids in the channels (22). In any case, it can be reasonably assumed that a PIP2 binding site must lie in a region closely apposed to the membrane. The polybasic region in the proximal C-terminal region of TRPV1 is located 22 amino acids after the bottom of the S6 (Fig. 1*B*). Thus, in addition to containing five basic residues and three hydrophobic residues, its location in the channel makes it an excellent candidate for binding directly to PIP2 in the plasma membrane.

To determine if the proximal C-terminal region is required for PIP2 regulation, we produced a number of deletions and neutralizations of multiple basic residues within and near our candidate PIP2 binding site. If PIP2 binding were eliminated by the deletions or mutations, we might expect either silent channels or channels that could not be opened using standard experimental protocols. Although deletion of the proximal C-terminal region and neutralization of >1 basic residue eliminated capsaicin-activated currents in our patches, we could not distinguish whether this was due to prevention of PIP2 binding to otherwise-normal channels or due to unrelated changes in protein folding, trafficking, or stability.

To determine if the proximal C-terminal region of TRPV1 could bind to PIP2 *in vitro*, we developed a FRET-based binding assay. The idea behind this assay was that a CFP fused to a fragment of TRPV1 might exhibit FRET upon binding to a commercially available PIP2 labeled with a green dye (TopFluor-PIP2). As shown in supplemental Fig. S1*A*, the emission spectrum of CFP overlaps with the excitation spectrum of TopFluor-PIP2, making CFP and TopFluor-PIP2 an ideal donor-acceptor pair for FRET.

We expressed the proximal C-terminal region of TRPV1 (amino acids 682–725) as a fusion protein to CFP in bacteria (TRPV1 682–725-CFP). We then lysed the bacteria and confirmed that the protein was soluble and monodispersed upon elution from a gel filtration column (data not shown). The emission spectrum of the soluble component of the bacterial lysate was then examined in a fluorometer. A typical emission spectrum of the TRPV1 682–725-CFP recorded in response to 415 nm light is shown in Fig. 6*A* (*black trace*). Adding TopFluor-PIP2 to TRPV1 682–725-CFP yielded robust FRET: the CFP signal markedly decreased and the TopFluor-PIP2 signal greatly increased (Fig. 6*A*). The amplitude of the increase in the TopFluor-PIP2 emission is evident upon comparison of the spectrum from TopFluor-PIP2 added to buffer (supplemental Fig. S1*B*, *red trace*) to TopFluor-PIP2 added to TRPV1 682–725-CFP (Fig. 6*A*, *red*). The direct excitation of TopFluor-PIP2 by the wavelength used to excite TRPV1 682–725-CFP, 415 nm,

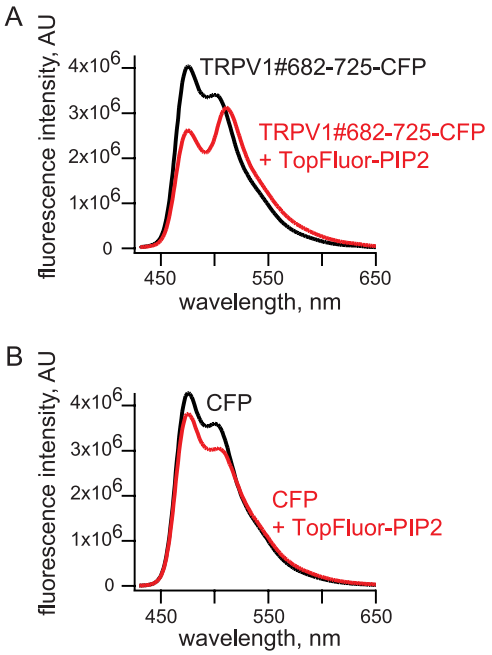


FIGURE 6. **PIP2 binds to the proximal C-terminal region of TRPV1 *in vitro*.** *A*, emission spectra in response to 415 nm excitation. The first data (*black trace*) collected was with lysate from bacteria expressing TRPV1 682–725-CFP in the cuvette. After addition of 6 $\mu$M TopFluor-PIP2, the measurements were repeated (*red trace*). *B*, emission spectra in response to 415 nm excitation. The first data (*black trace*) collected was with lysate from bacteria expressing CFP in the cuvette. After addition of 6 $\mu$M TopFluor-PIP2, the measurements were repeated (*red trace*).

cannot account for the increased TopFluor-PIP2 signal observed when added to TRPV1 682–725-CFP. In summary, using a proximal C-terminal fragment of TRPV1 as donor and PIP2 as an acceptor, significant FRET was observed. This FRET was not due to interaction of the PIP2 with CFP as CFP expressed in bacteria in the absence of a channel fragment did not participate in FRET with TopFluor-PIP2 (Fig. 6*B*). We conclude that, at least *in vitro*, PIP2 can interact directly with the proximal terminal region of TRPV1.

Ideally, we would like to examine whether the full-length C-terminal domain of TRPV1 interacts with PIP2 *in vitro*. However, we found that constructs that extended beyond amino acid 725 ran in the void of a size exclusion column (data not shown), indicating that the protein was aggregated. Protein from TRPV2, a closely related TRP channel (see alignment in Fig. 1*B*), was better behaved. We have previously shown that a construct corresponding to the near full-length C terminus (missing just the last seven amino acids) of TRPV2 ran as a monodispersed peak when run over a size exclusion column (23). When we repeated our *in vitro* FRET assay with TRPV2 645–753-CFP, we found that, like TRPV1 682–725-CFP, it interacted with TopFluor-PIP2 (supplemental Fig. S2). Given the similar role of PIP2 in regulating $Ca^{2+}$-dependent desensitization of both TRPV1 and TRPV2 (23), these data argue for conservation of mechanism among them.

## DISCUSSION

The TRP family of ion channels is composed of seven subfamilies, of which three have been reported to be potentiated by PIP2 (7, 24, 25). Their high expression levels in heterologous systems, activation by a water-soluble agonist, and lack of run down in patches from mammalian cells make TRPV1 an excellent candidate for addressing the molecular basis of PIP2 regulation. Here, we show that: 1) Pirt does not appear to influence regulation of TRPV1 by PIP2; 2) the distal C-terminal region of TRPV1 is not required for PIP2 regulation; and 3) the proximal C-terminal region of both TRPV1 and TRPV2 interacts with PIP2 *in vitro*.

One reason phosphoinositide regulation is so poorly understood is that definitive experimental approaches are lacking. For functional channels, we cannot control the composition of the lipid bilayer in cells or patches and can only vary the phosphoinositide concentration in a crude manner. Furthermore, given that many channels require PIP2 binding in order to function, mutations that disrupt PIP2 binding often yield functionally dead channels. When studying channel fragments, producing soluble, monodispersed protein has proven a major hurdle. Even once past that hurdle, binding studies with small, greasy molecules are not as straightforward as for studies of protein-protein interactions.

We find the Hilgemann model for phosphoinositide regulation of ion channels attractive (22). The binding site for phosphoinositides must be within a Debye length of the membrane, in at least one channel conformation, for an electrostatic interaction to occur. The simplest way this could occur is if one stretch of amino acids in a cytosolic domain constitutes the PIP2 binding site. The MARCKS protein, EGFR, and other proteins are believed to conform to this type of interaction (26). In contrast, the PIP2 binding site for inward rectifier $K^+$ channels seems to be more diffusely localized throughout the primary sequence of the protein. For these channels, the fold of the protein brings disparate regions of the primary sequence together to interface with the membrane (27, 28). Further experimentation will be required to learn whether the TRPV1 and TRPV2 PIP2 binding sites are restricted to a short stretch of amino acids in the proximal C-terminal region or whether, like inward rectifier channels, additional regions of sequence are involved. Given that the proximal C-terminal region is the most conserved cytosolic region among TRP channel families, it will also be interesting to see whether the mechanisms of lipid regulation are conserved among this family of channels with disparate functions.

Our data demonstrate that the integral membrane protein Pirt is not required for PIP2 regulation of TRPV1. This stands in marked contrast with previous work, which concluded that the enhancement of TRPV1 by PIP2 requires Pirt (16). The evidence that Pirt plays a role in temperature sensation and other TRPV1-related behaviors is strong. The latency time for $Pirt^{-/-}$ mice to withdraw their tails upon immersion into hot ($\geq$ 48 °C) water baths is significantly longer than that for wild-type mice. Injection of capsaicin into the hind paws of $Pirt^{-/-}$ mice lead to licking and biting of the hind paw, but for a significantly reduced duration than observed in wild-type mice.

Data indicating that Pirt did not alter channel gating is consistent with our own. Kim *et al.* measured $EC_{50}$ values for capsaicin activation of TRPV1 in HEK-293 neurons with and without Pirt, and found no difference (0.78 and 0.67 $\mu$M, respectively) (16). As shown in Fig. 4, we measured the $EC_{50}$ for

capsaicin activation of TRPV1 expressed in HEK-293 cells, and found no difference whether Pirt was (0.6 $\mu$M) or was not (0.4 $\mu$M) co-transfected in the cells. The other group also found that the threshold for heat activation of TRPV1 is not different in Pirt$^{-/-}$ mice compared with wild type, further indicating no effect of Pirt on TRPV1 gating properties. Interestingly, it was found that TRPV1 current densities were higher in wild-type mice than in Pirt$^{-/-}$ mice and also higher in HEK-293 cells stably expressing TRPV1 than in the same cell type transfected with Pirt (16). We did not address whether expression of TRPV1 was altered in either Pirt$^{-/-}$ mice or in HEK-293 cells transfected with TRPV1 but not with Pirt. The other group used surface biotinylation to compare the surface expression of TRPV1 in HEK-293 cells with and without Pirt, and they found no difference in the two cases (16). Nonetheless, it is possible that suppression of TRPV1 trafficking in the absence of Pirt could explain the nearly factor of 2 reduction in current density observed in Pirt$^{-/-}$ *versus* wild-type mice and HEK-293 cells without Pirt *versus* transfected with Pirt.

Our experimental approach focused on the effect of PIP2 on TRPV1 in the reduced system of excised patches. This allowed us to study direct effects of PIP2 in isolation of other pathways known to regulate TRPV1, including trafficking (7–8), phosphorylation (29–34), $Ca^{2+}$ (30, 33) and modulation through activation of RTKs (35) or GPCRs (6). Our solutions did not contain ATP or $Ca^{2+}$, and all the proposed models for the activation of TRPV1 by RTK and GPCR require the context of the whole cell. In contrast, previous work on Pirt used whole cell voltage clamp and was performed in the presence of extracellular $Ca^{2+}$ (the EGTA concentration in their intracellular solution did not eliminate $Ca^{2+}$ desensitization of TRPV1). It is possible that pathways intact in whole cells but disrupted in excised patches explain the differences in TRPV1 current density, temperature sensation and inflammatory hyperalgesia previously reported in the absence of Pirt. Indeed, TRPV1 currents in Pirt$^{-/-}$ cells were significantly less sensitive to activation by Bradykinin (a GPCR ligand) than wild-type cells (16).

Here we show that PolyK inhibits the capsaicin activated current in inside-out patches from both wild-type and Pirt$^{-/-}$ DRG neurons. In addition, we find that the apparent affinity of TRPV1 for PIP2 is not different in wild-type and Pirt$^{-/-}$ cells. Together with our data in HEK-293 cells, these results indicate that Pirt is not required for PIP2 regulation of TRPV1 in either HEK-293 cells or DRG neurons. Whether it plays a role in TRPV1 trafficking or in other aspects of TRPV1 function remains to be explored.

Does the proximal C-terminal region mediate regulation of TRPV1 by PIP2? Our data demonstrating a biochemical interaction hint that this may be the case but are not definitive. Historically, mutagenesis in combination with related ligands have been required to discern binding interactions. In the cyclic nucleotide-gated channel CNGA1, for example, the related ligands cAMP and cGMP are known to interact with the channels at the same site. Electrophysiological studies showed that cGMP is a full agonist and cAMP a weak partial agonist (36). A point mutation in the candidate cyclic nucleotide binding domain inverted the selectivity, making cGMP a partial agonist and cAMP a full agonist (37). This inversion of selectivity is much more powerful than a shift in the dose-response relation for just one agonist, as a change in $EC_{50}$ can arise from either a change in binding affinity or a change in the coupling between binding of agonist and the channel gating mechanism. Indeed, a shift in the $EC_{50}$ can even arise allosterically from nonspecific effects of the mutation on the channel gating mechanism (38). A change in selectivity, however, can arise only from mutations that alter the agonist binding site itself. Significant further study will be required before the PIP2 binding site responsible for PIP2 regulation can be definitively identified.

*Acknowledgments—We thank Dr. Xinzhong Dong for providing us with the mice used for this work and for his help with the genotyping of the animals. We are grateful to Dr. Françoise Haeseleer for husbanding and preparing mouse tissue. Thanks to Drs. Ivan F. Gonzalez, Bertil Hille, and William N. Zagotta for helpful discussions. We would also like to thank Mika Munari, Jennifer Cabarrus, Dr. Can Yuan, and Dr. Luis F. Santana for invaluable technical assistance.*

## REFERENCES

1. Tóth, A., Boczán, J., Kedei, N., Lizanecz, E., Bagi, Z., Papp, Z., Edes, I., Csiba, L., and Blumberg, P. M. (2005) *Brain Res. Mol. Brain Res.* **135,** 162–168
2. Caterina, M. J., Leffler, A., Malmberg, A. B., Martin, W. J., Trafton, J., Petersen-Zeitz, K. R., Koltzenburg, M., Basbaum, A. I., and Julius, D. (2000) *Science* **288,** 306–313
3. Binshtok, A. M., Bean, B. P., and Woolf, C. J. (2007) *Nature* **449,** 607–610
4. Wang, H., Ehnert, C., Brenner, G. J., and Woolf, C. J. (2006) *Biol. Chem.* **387,** 11–14
5. Pezet, S., and McMahon, S. B. (2006) *Annu. Rev. Neurosci.* **29,** 507–538
6. Chuang, H. H., Prescott, E. D., Kong, H., Shields, S., Jordt, S. E., Basbaum, A. I., Chao, M. V., and Julius, D. (2001) *Nature* **411,** 957–962
7. Stein, A. T., Ufret-Vincenty, C. A., Hua, L., Santana, L. F., and Gordon, S. E. (2006) *J. Gen. Physiol.* **128,** 509–522
8. Zhang, X., Huang, J., and McNaughton, P. A. (2005) *EMBO J.* **24,** 4211–4223
9. Zhu, W., and Oxford, G. S. (2007) *Mol. Cell Neurosci.* **34,** 689–700
10. Klein, R. M., Ufret-Vincenty, C. A., Hua, L., and Gordon, S. E. (2008) *J. Biol. Chem.* **283,** 26208–26216
11. Yao, J., and Qin, F. (2009) *PLoS Biol.* **7,** e46
12. Lukacs, V., Thyagarajan, B., Varnai, P., Balla, A., Balla, T., and Rohacs, T. (2007) *J. Neurosci.* **27,** 7070–7080
13. Suh, B. C., and Hille, B. (2005) *Curr. Opin. Neurobiol.* **15,** 370–378
14. Prescott, E. D., and Julius, D. (2003) *Science* **300,** 1284–1288
15. Brauchi, S., Orta, G., Mascayano, C., Salazar, M., Raddatz, N., Urbina, H., Rosenmann, E., Gonzalez-Nilo, F., and Latorre, R. (2007) *Proc. Natl. Acad. Sci. U.S.A.* **104,** 10246–10251
16. Kim, A. Y., Tang, Z., Liu, Q., Patel, K. N., Maag, D., Geng, Y., and Dong, X. (2008) *Cell* **133,** 475–485
17. Zacharias, D. A., Violin, J. D., Newton, A. C., and Tsien, R. Y. (2002) *Science* **296,** 913–916
18. Zheng, J. (2006) *Methods Mol. Biol.* **337,** 65–77
19. Patterson, G. H., Piston, D. W., and Barisas, B. G. (2000) *Anal. Biochem.* **284,** 438–440
20. Falkenburger, B. H., Jensen, J. B., and Hille, B. (2010) *J. Gen. Physiol.* **135,** 99–114
21. Shaner, N. C., Steinbach, P. A., and Tsien, R. Y. (2005) *Nat. Methods* **2,** 905–909
22. Hilgemann, D. W. (2004) *Science* **304,** 223–224
23. Mercado, J., Gordon-Shaag, A., Zagotta, W. N., and Gordon, S. E. (2010) *J. Neurosci.* **30,** 13338–13347
24. Rohács, T., Lopes, C. M., Michailidis, I., and Logothetis, D. E. (2005) *Nat. Neurosci.* **8,** 626–634
25. Zhang, Z., Okawa, H., Wang, Y., and Liman, E. R. (2005) *J. Biol. Chem.* **280,**

39185–39192
26. McLaughlin, S., Wang, J., Gambhir, A., and Murray, D. (2002) *Annu. Rev. Biophys. Biomol. Struct.* **31,** 151–175
27. Nishida, M., Cadene, M., Chait, B. T., and MacKinnon, R. (2007) *EMBO J.* **26,** 4005–4015
28. Haider, S., Tarasov, A. I., Craig, T. J., Sansom, M. S., and Ashcroft, F. M. (2007) *EMBO J.* **26,** 3749–3759
29. Bhave, G., Hu, H. J., Glauner, K. S., Zhu, W., Wang, H., Brasier, D. J., Oxford, G. S., and Gereau, R. W. t. (2003) *Proc. Natl. Acad. Sci. U.S.A.* **100,** 12480–12485
30. Docherty, R. J., Yeats, J. C., Bevan, S., and Boddeke, H. W. (1996) *Pflügers Archiv.* **431,** 828–837
31. Lee, S. Y., Lee, J. H., Kang, K. K., Hwang, S. Y., Choi, K. D., and Oh, U. (2005) *Arch. Pharm. Res.* **28,** 405–412
32. Mandadi, S., Numazaki, M., Tominaga, M., Bhat, M. B., Armati, P. J., and Roufogalis, B. D. (2004) *Cell Calcium* **35,** 471–478
33. Rosenbaum, T., Gordon-Shaag, A., Munari, M., and Gordon, S. E. (2004) *J. Gen. Physiol.* **123,** 53–62
34. Sikand, P., and Premkumar, L. S. (2007) *J. Physiol.* **581,** 631–647
35. Bonnington, J. K., and McNaughton, P. A. (2003) *J. Physiol.* **551,** 433–446
36. Gordon, S. E., and Zagotta, W. N. (1995) *Neuron* **14,** 177–183
37. Varnum, M. D., Black, K. D., and Zagotta, W. N. (1995) *Neuron* **15,** 619–625
38. Gordon, S. E., and Zagotta, W. N. (1995) *Neuron* **14,** 857–864